Optimizing the Euclid Figure of Merit for SPV3 Fisher Matrix Forecasts

Vincenzo F. Cardone[1], I. Tutusaus, M. Carbone, D. Sapone

The present document summarizes the results of a preliminary analysis carried on to investigate which is the miniman number of redshift bins needed to achieve a Figure of Merit (FoM) larger than the requirement value set in the RedBook, $\mathrm{FoM_{RB}} = 400$, using Euclid photometric and spectroscopic[2] probes only. We remember that this number refers to the case where flatness is not imposed a priori so that the full list of cosmological parameters read

$$\mathbf{p}_{cosmo} = \{\Omega_M, \Omega_X, \Omega_b, w_0, w_a, h, n_s, \sigma_8\}$$

with Ω_i the present day density parameters of total matter (M), dark energy (X), and baryons (b), (w_0, w_a) the two parameters of the CPL model for the dark energy equation of state, h the Hubble constant in units of 100 km/s/Mpc, n_s the slope of the primordial perturbation, and σ_8 the variance of linear perturbations on scale $8h^{-1}$ Mpc. We set their fiducial values as in the IST:F paper, i.e.

$$\mathbf{p}^{fid}_{cosmo} = \{0.32, 0.68, 0.05, -1.0, 0.0, 0.67, 0.96, 0.816\} \ ,$$

while the sum of neutrino masses is set to 0.06 eV and held fixed in the analysis.

1 Working assumptions

The main aim of the present analysis is to revisit the choice of 13 redshift bins as minimal number to get $FoM \geq 400$. Such a check is needed since both the survey specifics, and the theoretical modeling have changed. Moreover, the way systematics are taken into account is also different. On the other hand, not all the informations available during the SPV2 period are still at disposal so that repeating the same analysis in all its steps is not possible. We will therefore carry on our investigation according to the following schematic strategy.

1. We first adopt the same forecasts recipe used in IST:F and SPV2, but changing both the assumptions on the redshift distribution $n_i(z)$ of each bin and the galaxy bias, and the survey specifics for the total survey area $\mathcal{A}_{surv}$ and the intrinsic ellipticity dispersion σ_ϵ. This test will update the SPV2 results taken care of how our knowledge of the survey has changed in the recent years. The outcome of this analysis will be a first answer to the question about the number of bins needed to achieve the FoM goal.

2. We then move to the more recent recipe which is implemented in the v2 of the likelihood code `CLOE` (Cosmology Likelihood of Observables in Euclid).

[1]corresponding author: `vincenzo.cardone@inaf.it`

[2]Although not obtained by Euclid data, we will sometimes include in the spectroscopic probes also a prior based on the results of the BOSS survey. This is to account for the change in the redshift range originally proposed for the spectroscopic survey due to the consideration that the BOSS data were already available. The BOSS contribution is, however, subdominant.

This step forward is necessary in order to allow a more direct comparison with future MCMC based forecasts which will be available when `CLOE v2` will be released. Moreover, this new recipe includes additional terms in the harmonic power spectra which can not be neglected in order to avoid biased constraints on cosmological parameters.

3. All the above steps are carried out under the *optimistic* scenario (which we will detail later). For a subset of the cases considered above bracketing the preferred one, we will repeat the analysis to investigate how the FoM changes if some assumptions or part of the data vector are dropped out.

Although we do not give here the details of the Fisher matrix implementation and of the recipes adopted (referring the interested reader to the extensive description in the IST:F paper and the `CLOE v2` documentation), it is nevertheless worth reminding below the main assumptions.

i. The nonlinear matter power spectrum is computed using the same TakaBird recipe adopted in IST:F, while a deterministic linear bias is used to get the matter - galaxy and galaxy - galaxy cross power spectra; we do not account for the impact of baryons on the power spectra in the fiducial analysis, but we will investigate it when considering deviations from the reference assumptions.

ii. The galaxy bias is taken constant in each tomographic bin with fiducial values set according to what has been measured on Flagship mock data; this is different from what has been done in IST:F and extended forecast papers since there the bias was taken to be piecewise constant assuming the true redshift were known; the present analysis is more realistic and in agreement with what is done when dealing with actual data.

iii. The eNLA model is used for the intrinsic alignment (IA) power spectra allowing for a dependence on the luminosity; although this is likely redundant and will be abandoned in MCMC forecasts, we prefer to still include it in order to ease the comparison with previous results.

iv. The covariance matrix for the photometric probes is computed analytically using as default case the Gaussian component only; we will nevertheless investigate the impact of SSC in a final step.

A further difference with respect to the IST:F and SPV2 analysis is in how we deal with the cut on the data vector. We start with the full multipole range $(\ell_{min}, \ell_{max}) = (10, 5000)$ which we split in 32 logarithmically spaced bins. The centre of each bin is set as $\ell_{c,i} = [\mathrm{dex}(\lambda_{i+1}) + \mathrm{dex}(\lambda_i)]/2$, while the width is simply $\Delta\ell_i = [\mathrm{dex}(\lambda_{i+1}) - \mathrm{dex}(\lambda_i)]$, with $\lambda_i = \log \ell_i$ and ℓ_i the lower limit of the i - th bin. We then arrange the elements of the full 3x2pt data vector as follows

$$
\begin{aligned}
\mathcal{D}_{\rm 3x2pt} \;=\; \big\{ & C_{ij}^{LL}(\ell_1) \;\; \text{with } i \text{ from 1 to } \mathcal{N}_{WL} \text{ and } j \text{ from } i \text{ to } \mathcal{N}_{WL} \\
& C_{ij}^{GL}(\ell_1) \;\; \text{with } i \text{ from 1 to } \mathcal{N}_{GC} \text{ and } j \text{ from 1 to } \mathcal{N}_{WL} \\
& C_{ij}^{GG}(\ell_1) \;\; \text{with } i \text{ from 1 to } \mathcal{N}_{GC} \text{ and } j \text{ from } i \text{ to } \mathcal{N}_{GC} \\
& C_{ij}^{LL}(\ell_2) \;\; \text{with } i \text{ from 1 to } \mathcal{N}_{WL} \text{ and } j \text{ from } i \text{ to } \mathcal{N}_{WL} \\
& C_{ij}^{GL}(\ell_2) \;\; \text{with } i \text{ from 1 to } \mathcal{N}_{GC} \text{ and } j \text{ from 1 to } \mathcal{N}_{WL} \\
& C_{ij}^{GG}(\ell_2) \;\; \text{with } i \text{ from 1 to } \mathcal{N}_{GC} \text{ and } j \text{ from } i \text{ to } \mathcal{N}_{GC} \\
& \ldots\ldots\ldots\ldots \\
& \ldots\ldots\ldots\ldots \\
& \ldots\ldots\ldots\ldots \\
& C_{ij}^{LL}(\ell_{max}^{GC}) \;\; \text{with } i \text{ from 1 to } \mathcal{N}_{WL} \text{ and } j \text{ from } i \text{ to } \mathcal{N}_{WL} \\
& C_{ij}^{GL}(\ell_{max}^{GC}) \;\; \text{with } i \text{ from 1 to } \mathcal{N}_{GC} \text{ and } j \text{ from 1 to } \mathcal{N}_{WL} \\
& C_{ij}^{GG}(\ell_{max}^{GC}) \;\; \text{with } i \text{ from 1 to } \mathcal{N}_{GC} \text{ and } j \text{ from } i \text{ to } \mathcal{N}_{GC} \big\} \quad (1)
\end{aligned}
$$

where $C_{ij}^{AB}(\ell)$ are the tomographic harmonic power spectra for shear - shear ($A = B = L$), position - shear ($A = G, B = L$), and position - position ($A = B = G$) correlation, also referred to in the following with the acronyms WL (weak lensing), GGL (galaxy - galaxy lensing[3]), and GCph, (photometric galaxy clustering) respectively. All the multipole bins with $\ell_{c,i} \leq \ell_{max}^{GC}$ are included in $\mathcal{D}_{\rm 3x2pt}$. However, it is custormary to push WL to larger ℓ_{max} so that the condition $\ell_{c,i} \leq \ell_{max}^{WL}$ will select some few more multipole bins where WL data only are used. We collect them in a data vector constructed arranged as in (1), but only containing WL data for the bins with $\ell_{max}^{GC} < \ell_{c,i} \leq \ell_{max}^{WL}$. We denote this data vector as $\mathcal{D}_{\rm WLA}$. We can similarly build two additional data vectors denoted as $\mathcal{D}_{\rm WLO}$ and $\mathcal{D}_{\rm GCO}$ made out by WL and GCph data only from multipole bins up to ℓ_{max}^{WL} and ℓ_{max}^{GC}, respectively. In the forecast analysis, we will consider four scenarios labelled as follow according to which data vector $\mathcal{D}$ is used, namely :

$$
\mathcal{D} = \begin{cases}
\mathcal{D}_{\rm WLO} & \text{WL only (WLO)} \\
\mathcal{D}_{\rm GCO} & \text{GCph only(GCO)} \\
\mathcal{D}_{\rm 3x2pt} & \text{3x2pt (3x2)} \\
\mathcal{D}_{\rm 3x2pt} \cup \mathcal{D}_{\rm WLA} & \text{all photo probes (All)}
\end{cases} .
$$

In the following, we will consider the *optimistic* scenario setting

$$
\ell_{max}^{WL} = 5000 \;\; , \;\; \ell_{max}^{GC} = 3000 \;\; ,
$$

but we will investigate also the impact of making more severe cuts. Finally, although this assumption would likely be changed in the future, we will keep assuming that the source and lens samples are the same so that the redshift

[3] In IST:F and SPV2, this term was referred to as XC for cross - correlation, but we prefer here to adopt the nomenclature currently used in the literature.

distributions are identical, and the same number of redshift bins is used for both WL and GCph, i.e., $\mathcal{N}_{WL} = \mathcal{N}_{GC} = \mathcal{N}_z$.

We will investigate how the results depend on both the number of bins $\mathcal{N}_{bin}$, and their type, i.e., whether they are chosen to be equipopulated (that is to say, with variable width set in such a way that the number density of galaxies is the same in all bins) or equidistant (hence with fixed width so that each bin has its specific number density). We update three important survey specifics as follows

$$\begin{cases} \mathcal{A}_{surv} = \text{total survey area} = 14000 \text{ sq deg} \\ \\ n_g = \text{total galaxy number density} = 28.73 \text{ gal/arcmin}^2 \\ \\ \sigma_\epsilon = \text{intrinsic ellipticity dispersion} = 0.26\sqrt{2} = 0.37 \end{cases} ,$$

which are in agreement with most recent information on these quantities.

1.1 Nuisance parameters

Each survey aims at constraining cosmological parameters. Unfortunately, these are hidden behind a curtain made of a cloud of additional quantities which are needed to compute the theoretical predictions for each probe the data measure. With an abuse of terminology, we will collectively refer to all these non cosmological quantities as *nuisance parameters*. They are very different in nature and nurture, but all share the same basic feature: they must be marginalized over in order to quantify the error on the cosmological parameters. We briefly discuss below the ones we include in our analysis.

Intrinsic Alignment. This is the first example of *nuisance* parameters which are actually *astrophysical* parameters since they carry information on galaxies formation scenarios. As yet said above, we use the eNLA model for IA which is assigned by the three parameters $\mathbf{p}_{IA} = \{\mathcal{A}_{IA}, \eta_{IA}, \beta_{IA}\}$. These quantities give the IA amplitude at a reference point, and its scaling with redshfit and luminosity. Fiducial values are as in the IST:F paper.

Galaxy bias. Under our assumption of linear deterministic bias, these quantities set, at each redshift, the relative amplitude of the galaxy - galaxy power spectrum with respect to the matter one. We take them as constant in each tomographic bins so that we must add $\mathcal{N}_{GC}$ nuisance parameters to the full list. The fiducial values are set in agreement with what has been measured after selecting a photometric clustering sample making a magnitude cut on galaxies in the Flagship catalog.

Magnification bias. In `CLOE v2` recipe, the impact of magnification on the number counts is taken into account by adding the relevant contribution to the GCph and GGL harmonic spectra. As for the galaxy bias, we assume that the magnification bias is constant in each tomographic bin so that we must add other $\mathcal{N}_{GC}$ nuisance parameters if `CLOE v2` recipe is used in the forecast. To fix their fiducial values, we consider the case in which magnification bias only changes the apparent magntiude of a

galaxy thus altering the number density pushing some objects above the detection threshold. In this case, the magnification bias for the i-,th bin is $b_{M,i} = 5s_i - 2$, where s_i is the mean logarithmic slope of the galaxy number density vs limiting magnitude relation. An analytical fit to $s(z)$ measured using Flagship galaxy samples has been recently provided. We use this relation to compute $b_{M,i} = 5s_{fit}(z_i) - 2$ with z_i the mean redshift of the i-th bin. Note that we prefer to use $b_{M,i}$ rather than $s_i = s(z_i)$ as nuisance parameters in order to allow for an effective magnification bias hence accounting for deviations from the $b_M(z) - s(z)$ relation.

Shear multiplicative bias. Shape measurement algorithms have made enormous progress from the epoch of Stage I lensing surveys yet they are still not perfect. The errors are, however, so small that a linear fit is sufficient to model the relation between the actual shear and the measured one. This induces a systematics on the lensing power spectra which can be taken into account introducing a shear multiplicative bias and an additive one. Assuming this latter to be negligible or corrected for at the data production level[4], we are left with the multiplicative bias m only. Following typical analyses in literature, we will model it as constant in each bin thus adding $\mathcal{N}_{WL}$ nuisance parameters to the full parameters list. We set $m_i = 0$ as fiducial value since the Euclid requirement is $|m| \leq 1.5 \times 10^{-3}$.

Photo-z systematics. The large number of galaxies in the imaging sample makes it impossible to perform spectroscopic measurement of their redshifts. Lensing surveys therefore rely on photometric redshift techiniques which must be accurate enough to not bias the determination of the redshift distribution $n_i(z)$ of each bin. To the lowest level, this is accounted for replacing the actual redshift distribution with an effective one given by $n_i^{eff}(z) = n_i(z - \Delta z_i)$ where Δz_i is a nuisance parameter to be marginalised over in each bin. Since we are assuming that WL and GCph use the same sample of galaxies and number of bins, we have $\mathcal{N}_{bin}$ additional nuisance parameters Δz_i. We take as fiducial value $\Delta z_i = 0$ in accordance with the requirement $\Delta z_i \leq 0.005(1 + z_i)$ with z_i the mean bin redshift. Note that, should we use two different samples for WL and GCph, the number of nuisance parameters would increase to $\mathcal{N}_{WL} + \mathcal{N}_{GC}$ since we can not assume a priori that $\Delta z_i^{WL} = \Delta z_i^{GC}$.

It is worth noticing that, neglecting magnification and assuming the same sample for WL and GCph, the total number of nuisance parameters is

$$\mathcal{N}_{np} = 3 + \mathcal{N}_{bin} + \mathcal{N}_{bin} + \mathcal{N}_{bin} = 3(\mathcal{N}_{bin} + 1) \tag{2}$$

which increases to

$$\mathcal{N}_{np} = 3 + \mathcal{N}_{bin} + \mathcal{N}_{bin} + \mathcal{N}_{bin} + \mathcal{N}_{bin} = 4\mathcal{N}_{bin} + 3 \tag{3}$$

if magnification bias is included. In the most general case, with magnification included and two separate samples for WL and GCph, the number of nuisance parameters is

[4]This assumption will be dropped in the next-to-come recipe.

$$\mathcal{N}_{np} = 3 + \mathcal{N}_{GC} + \mathcal{N}_{GC} + \mathcal{N}_{WL} + \mathcal{N}_{WL} + \mathcal{N}_{GC} = 3\mathcal{N}_{GC} + 2\mathcal{N}_{WL} + 3 \ . \quad (4)$$

Using 10 redshift bins as an example, we thus have $(33, 43, 53)$ nuisance parameters to be marginalised over depending on the recipe and sample assumptions. Needless to say, such a large number of nuisance parameters degrade the constraints on the cosmological parameter so that one typically tries to add priors based on preliminary constraints on systematics. In the Fisher matrix formalism, this is achieved adding to the probe Fisher matrices a prior one which we will denote as $\mathbf{\Pi}$. This is $\mathcal{N}_\theta \times \mathcal{N}_\theta$ diagonal matrix with $\mathcal{N}_\theta = \mathcal{N}_{cosmo} + \mathcal{N}_{np}$ the total number of cosmological and nuisance parameters.

We will set its diagonal elements according to the following rules

$$\Pi_{ii} = \begin{cases} 0 & \text{if } i \text{ refers to cosmological parameters} \\ 0 & \text{if } i \text{ refers to IA parameters} \\ 0 & \text{if } i \text{ refers to galaxy bias} \\ \left(\varepsilon_M |b_{M,i}^{fid}|\right)^{-2} & \text{if } i \text{ refers to magnification bias} \\ \left(\varepsilon_m \sigma_m^{fid}\right)^{-2} & \text{if } i \text{ refers to shear multiplicative bias} \\ \left[\varepsilon_z \sigma_z^{fid}(1+z_i)\right]^{-2} & \text{if } i \text{ refers to photo} - \text{z mean shift} \end{cases} \quad (5)$$

with

$$\sigma_m^{fid} = 1.5 \times 10^{-3} \ \ , \ \ \sigma_z^{fid} = 0.005 \ \ ,$$

and $(\infty, \varepsilon_m, \varepsilon_z)$ set to $(0, 1, 1)$ in the reference scenario[5]. These quantities are then varied to investigate how the constraints on cosmological parameters change depending on the priors on the nuisance ones.

1.2 Differences with respect to previous forecasts

This is not the first time forecasts for Euclid are presented. In particular, two well known examples are the IST:F and the SPV2 ones. There is also a less well known case which we refer to as SPV2+ which has been produced after the nominal end of the SPV2 with the aim of extending that analysis including additional cases. This has not been published, but it is described in a technical note available on request to the corresponding author.

In the first part of the present analysis, we will keep using the same recipe adopted for both IST:F and SPV2. Nevertheless, there are some differences in the input quantities and survey specifics which impact the final forecasts. We briefly describe them in the following.

[5]Note that we set $\varepsilon_M = \infty$ as reference case just as a formal way to say that we do not put any prior on the magnification bias parameters.

Redshift distributions. We still assume that the WL and GCph samples are the same so that we also use the same number of redshift bins in the tomographic analysis. However, the number density of each bin as function of redshift, $n_i(z)$ is not the same for IST:F, SPV2, and SPV3 (that is how we will refer to the present analysys hereafter). In IST:F, we convolved a model for the intrinsic redshift distribution $n(z)$ with the photo-z pdf modeled as the sum of two Gaussians with parameters equal for all bins. A step forward has been made in SPV2 and SPV2+ fitting the Gaussian parameters to mock dataset to account for the different photo-z quality of each bin. Here, we use the $n_i(z)$ function obtained using a photo-z method to galaxy samples exctracted from the Flagship simulation after perfroming a magnitude cut to mimic the Euclid selection strategy.

Bin spacing. There are two possible strategies to divide galaxies in redshift bins. First, one can perform the splitting in such a way that the same number of galaxies is present in each bin. As a consequence, each bin will have a different width with the higher redshift ones being larger to compensate for the asymmetry of the total redshift distribution. On the contrary, one can fix the width of the bins so that each bin will have a different number of galaxies in it. We will refer to these two cases as equipolulated (EP) and equidistant (ED). EP bins have been used in IST:F and SPV2, while the impact of changing from EP to ED has been investigated in SPV2+. We repeat here this latter analysis considering both EP and ED bins.

Number of multipole bins. Both in IST:F and SPV2, optimisitc and pessimistic scenarios were considered with the difference being set by the maximum multipole used in WLO and 3x2pt Fisher forecasts. However, once the ℓ range has been set, the same number of multipole bins was used so that the data vector has the same length in both scenarios. The dependence on the number of multipole bins was then investigated in SPV2+ who also considered the impact of increasing the minimum ℓ. On the contrary, here, we hold fixed to 32 the number of multipole bins and cut the optimistic data vector and covariance matrix to get a pessimistic one. However, this difference is not expected to have a dramatic impact based on what we have found in SPV2+ where we have shown that the forecasts were independent on the number of ℓ bins as this becomes larger than 30.

GCsp Fisher matrix. The recipe for the spectroscopic data is the same as for the previous forecasts. However, there are already differences between IST:F and SPV2/SPV2+ because of the different versions of the spectroscopic sample redshift distribution. As an additional ingredient, we now marginalise over the purity of the sample according to the recipe recently developed by the P&C taskforce to account for uncertainties on this quantity. In order to be conservative, we moreover only consider the case with $k_{max} = 0.25h/\mathrm{Mpc}$ as upper limit to the GCsp data.

Survey specifics. Three main numbers related to the survey have been changed with respect to the IST:F and SPV2 forecasts. The survey area $\mathcal{A}_{surv}$

is reduced from 15000 to 14000 sq deg, while the intrinsic ellipticity dispersion σ_ϵ is raised from 0.21 to 0.26 per component. A minor change has also occured for the the total number density n_g which is reduced from 30 to 28.72 gal/arcmin^2. Considering that the FoM scales with $(\mathcal{A}_{surv}, 1/\sigma_\epsilon, 1/\sqrt{n_g})$, all these changes are expected to decrease the FoM. However, part of this decrement can be compensated by a possible improvement in the photo - z quality.

Systematics. IST:F did not include any kind of systematics apart for the impact of photo - z whose parameters were however held fixed. In SPV2/SPV2+, a step forward has been made writing the full Fisher matrix as

$$\mathbf{F}_{tot} = f_{sys}^2 \left(\frac{\mathcal{A}_N \mathbf{F}_{LN}}{\mathcal{A}_N + \mathcal{A}_S} + \frac{\mathcal{A}_S \mathbf{F}_{LS}}{\mathcal{A}_N + \mathcal{A}_S} \right) + \mathbf{F}_{GC} + \mathbf{F}_{BOSS} \tag{6}$$

where $\mathbf{F}_{LN}$ and $\mathbf{F}_{LS}$ are the WL + GCph + GGL Fisher matrices for the North and South region of the survey computed for a total area $\mathcal{A}_N + \mathcal{A}_S = 15000$ sq deg and scaled to the corresponding areas, $\mathbf{F}_{GC}$ is the GCsp Fisher matrix, and $\mathbf{F}_{BOSS}$ is a prior coming from BOSS data. The multiplicative factor f_{sys} was introduced by hand to qualitatively account for the expected degradation of the FoM due to increase in the number of nuisance parameters related to systematics. Its value was set in such a way to reproduce what was available in the literature and in some preliminary tests. IST:F is recovered from (6) setting

$$\mathbf{F}_{LN} = \mathbf{F}_{LS} \quad , \quad f_{sys} = 1 \quad , \quad \mathbf{F}_{BOSS} = 0 \quad . \tag{7}$$

These same rules are adopted here to get what we will refer to as the *Euclid only* (EuO) case, while we call *Euclid* (Euc) the case with the BOSS prior included (i.e., with $\mathbf{F}_{BOSS} \neq 0$). However, we stress that now the dimension of the total Fisher matrix $\mathcal{F}_{tot}$ is much larger than in the IST:F case since we now explicitly account for all the nuisance parameters listed before each one introduced with its own recipe (which were not available at the SPV2/SPV2+ epoch).

As a final remark, we want to comment on the forecast codes used for the analysis. The GCsp Fisher matrix and the BOSS prior have been obtained using `SOAPFish` developed by D. Sapone, and validated during the IST:F challenge. The different treatment of systematics and the need to implement the `CLOE v2` recipe for later forecasts prevented us from using `STAFF` as done for SPV2. We are now using the new code `LiFE` (Likelihood and Forecasts for Euclid) developed, as `STAFF`, by V.F. Cardone. Being an extension of `STAFF`, it was expected that `LiFE` reproduces the IST:F results when the same recipe and input are used. This is indeed the case so we consider `LiFE` successfully passing the IST:F validation so that its results are trustworthy.

2 FoM optimization under the IST:F recipe

Let us now move to the core of our analysis by investigating how the forecasts depend on the number and spacing of redshift bins. In this section, we keep using

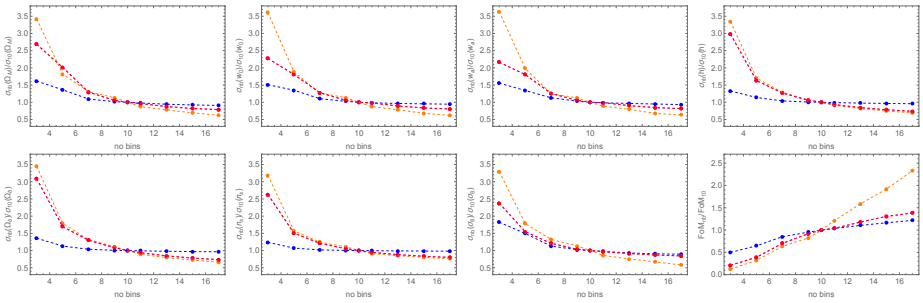

Figure 1: Errors on the cosmological parameters of a flat GR model and FoM as a function of the number of bins normalised with respect to the results for $\mathcal{N}_{bin} = 10$. Blue, orange, magenta, red lines refer to WLO, GCO, 3x2, All cases, respectively, according to the terminology explained in the text. Note that 3x2 and All cases almost perfectly match so that the magenta lines are not visible since because of overlap with the red ones. Hereafter, the dots are the cases actually computed, while dashed lines are only meant to guide the eye.

the IST:F recipe to easy the comparison with previous results alwasy taking in mind, however, the differences discussed in the previous paragraph. As yet said before, we will assume that the source (WL) and lens (GCph) samples are the same so that the numbers of WL and GCph bins are equal too, i.e., we set $\mathcal{N}_{WL} = \mathcal{N}_{GC} = \mathcal{N}_{bin}$. This is the quantity we vary in the rest of this section.

2.1 Dependence on the number of redshift bins

Increasing $\mathcal{N}_{bin}$ has two opposite effects on the constraints. First, a finer binning allows for a better tomographic analysis more carefully tracing the evolution of the dark energy equation of state and of the other quantities of interest. It also increases the length of the data vector hence the effective number of degrees of freedom which typically helps in narrowing down the constraints on cosmological parameters. Eqs.(2) - (3), however, show that the number of nuisance parameters quickly increases too as $\mathcal{N}_{bin}$ gets larger. More nuisance parameters mean more degeneracy in the multidimensional parameter space with the need to marginialise over a lot of quantities hence decreasing the constraining power.

Which duelist is the winning one depend on the probe at hand. This is shown in Fig. 1 where we plot the marginalised errors on the cosmological parameters for a flat GR model normalised with respect to the case with $\mathcal{N}_{bin} = 10$ taking the bins to be equipopulated. Different colored lines refer to different probe combinations. While the overall trend is the same, the quantitative one is different with the number of bins having a larger impact for GCO and a minimal one for WLO. This is because GCO is the less constraining probe hence increasing the amount of information has a stronger effect. On the contrary, the two oppoiste effects quoted above almost compensate each other for WLO, while the situation is intermediate when both probes and their cross - corrleation are used. As a net result, the FoM keeps increasing with $\mathcal{N}_{bin}$ for GCO, but tends to flatten for the other cases as shown in the rightmost bottom panel.

Fig. 1 refers to the case with no priors added on systematics parameters before marginalising over them. We have repeated the same analysis using

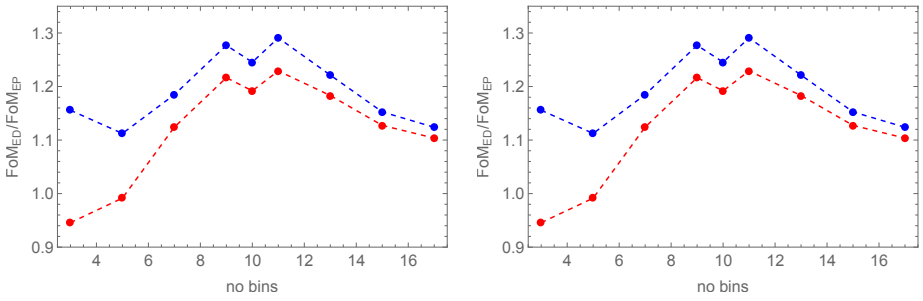

Figure 2: $\mathrm{FoM_{ED}}/\mathrm{FoM_{EP}}$ ratio as a function of the number of bins for a non flat GR model. Blue and red lines refer to the All and Euc cases, while left and right panels are for the cases when marginalization over nuisance parameters is performed without or with fiducial priors on systematics.

fiducial priors, and find out qualitatively consistent results. Roughly speaking, this is because we are plotting ratio of errors so that priors act in the same way on both numerator and denominator hence nearly dropping out of the ratio. Actually, the results are quantitatively smaller with the number on the y-axes in the plot being closer to unity. However, the curves only become nearly flat if we make the priors so strong that the total Fisher matrix becomes priors dominated which will never happen in practice.

Finally, we have performed the same check using equidistant rather than equipopulated bins or dropping out the flatness and/or GR assumptions finding qualitatively consistent trends. Hereafter, we will only focus on the FoM since this is the quantity we are most interested in.

2.2 Dependence on the redshift binning strategy

Let us now investigate whether the binning strategy impact the forecasts. Fig. 2 shows the ratio $\mathrm{FoM_{ED}}/\mathrm{FoM_{EP}}$ with $\mathrm{FoM_{ED}}$ ($\mathrm{FoM_{EP}}$) the FoM for non flat GR models computed using equidistant (equipopulated) redshift bins. We consider both the case when all photometric probes are used (referred to as All) and when GCsp and BOSS are included (dubbes as Euc). We marginalise over all nuisance parameters without (left) or with (right) priors on systematics finding a hardly visible difference. For all these combinations, we get that ED bins perform better than EP ones as soon as $\mathcal{N}_{bins} \geq 5$. As expected, the effect is larger for the All rather than for Euc case since, in the second configuration, one is including spectroscopic probes which are independent on both the number of bins and the way they are defined. It is also worth noticing how the effect is non monotonic with the ratio $\mathrm{FoM_{ED}}/\mathrm{FoM_{EP}}$ approaching unity as $\mathcal{N}_{bin}$ gets larger. Explaining this behaviour is the aim of the rest of this subsection.

As a first guess, one could argue that ED bins perform better because the corresponding dataset has a larger S/N. To check this hypothesis, we plot in Fig. 3 the total S/N defined as

$$\nu_{tot} = \left(\mathcal{D}^T \cdot \Psi \cdot \mathcal{D}\right)^{1/2} \tag{8}$$

where $\Psi = \mathrm{Cov}^{-1}$ is the precision matrix, and Cov the analytic Gaussian only covariance matrix. Somewhat surprisingly, the ED bins have an overall smaller

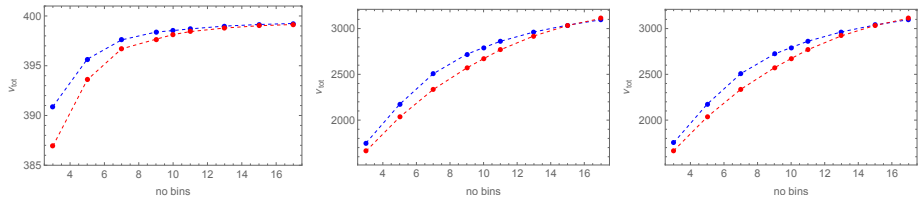

Figure 3: Total S/N ratio as a function of number of bins for EP (blue) and ED (red) bins. Left, centre, and right panels refer to WLO, GCO, All datasets.

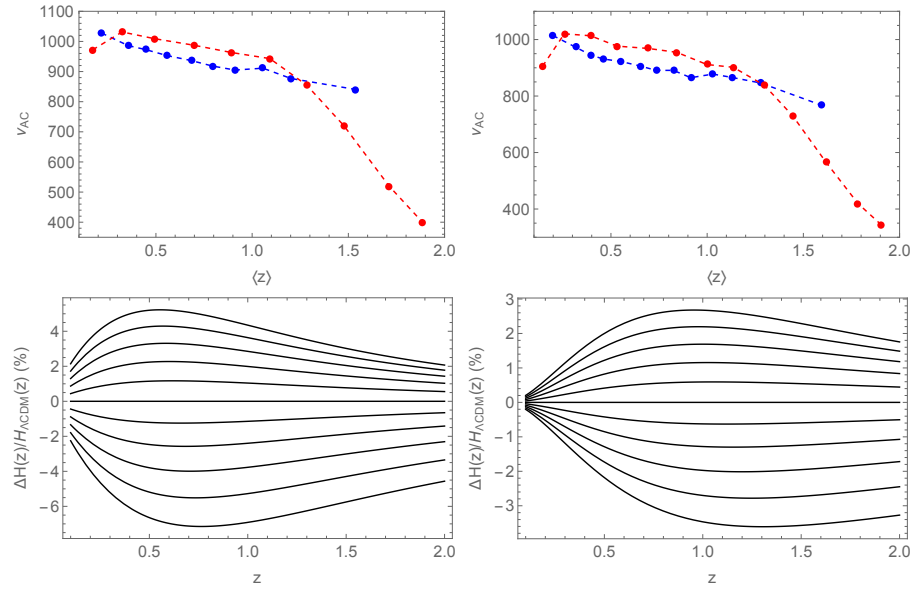

Figure 4: *Top.* Autocorrelation S/N ratio vs the mean bin redshift for EP (blue) and ED (red) bins using the All dataset split in 10 (left) or 13 (right) bins. *Bottom.* Percentage deviation of the Hubble rate $H(z)$ from the ΛCDM model setting all parameters to their fiducial values but w_0 (left) or w_a (right).

S/N, no matter whether one uses WL and GCph data separately or combined in the full 3x2pt analysis. The difference becomes less and less important as one moves to larger number of bins which is in accordance with the FoM ratio trend in the high $\mathcal{N}_{bin}$ regime shown before.

Actually, the total S/N compresses all the information into a single number hence making difficult to understand what is going on. As an alternative, we therefore introduce the following quantity

$$\nu_{AC} = \left(\mathcal{D}_{AC}^{T} \cdot \Psi_{AC} \cdot \mathcal{D}_{AC}\right)^{1/2} \tag{9}$$

where $\mathcal{D}_{AC}$ contains only data vector elements of the form $C_{ii}^{AB}(\ell)$, i.e., it only refers to quantities (either WL, GCph, or GGL ones) correlated within the same redshift bin. As such, ν_{AC} is actually a function of the redshift as we show in top panels of Fig. 4 where we plot it for the All dataset vs the mean redshift of the bin for the case with 10 (left) and 13 (right) bins. It is now evident that

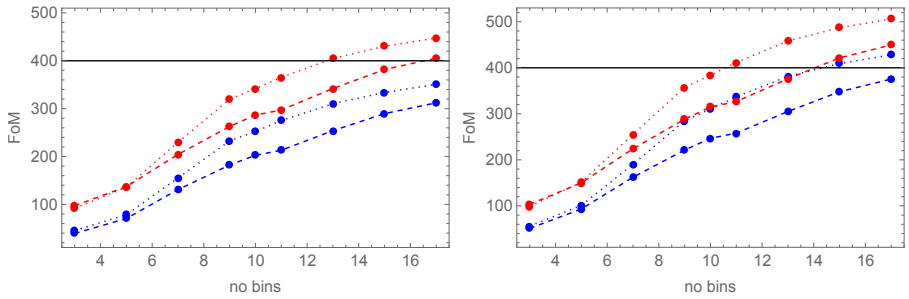

Figure 5: FoM as function of the number of bins for a non flat GR model. Blue and red lines refer to the All and Euc datasets with dashed and dotted lines for EP and ED bins. In the left panel, nuisance parameters are marginalised over without any prior, while fiducial priors are used in the right one.

ED bins have indeed a larger ν_{AC} in the bins which probe the redshift range $(0.2, 1.2)$ because of the larger number of galaxies in each bin. It is instructive to also look at the bottom panels where we show, as an example, the percentage deviation of the Hubble expansion rate $H(z)$ from the fiducial ΛCDM model for different set of parameters. In particular, we vary w_0 from -1.25 to -0.75 in steps of 0.05 (from top to bottom curves) in the left panel, and w_a from -0.5 to 0.5 in steps of 0.1 (from bottom to top curves) in the right one. It is eviden that ED bins have larger ν_{AC} values right over the same redshift range where the dependence of cosmological quantities on the model parameters is stronger. Adding more bins at larger z has then a minor impact explaining why ED perform better even if their total S/N is smaller due to the presence of the last bins which have a very small S/N.

Although ν_{AC} is only a part of the total S/N, a similar argument (yet more complicated) can be done for the cross-correlation among different redshift bins. We can qualitatively say that how the total S/N budget is invested is more important than how large it is. This argument allows to explain the FoM trends in Fig. 2 hence pointing at ED as the best binning strategy.

2.3 Optimal FoM and requirements on priors

The reader in hurry would have probably preferred to skip the previous subsections to directly arrive to the answer one is most interested in. That is to say, understanding whether Euclid is able to fulfil the requirement on the FoM computed for a non flat CPL model. This is shown in Fig. 5 where the FoM as a function of the number of bins is plotted. Looking at the horizontal line which marks the requirement, we conclude that the minimal condition to get FoM ≥ 400 is using 13 ED redshift bins. For this configuration, we indeed get FoM $= 405$ which reduces to FoM $= 342$ if 13 EP bins are used. One could wonder why we get a FoM smaller than the requirement using 13 EP bins, while this was the recommended choice at the end of SPV2 analysis. Actually, this difference is entirely due to the changes in the survey specifics. Indeed, it is

$$\frac{\text{FoM(SPV3)}}{\text{FoM(SPV2)}} \simeq \left[\frac{\mathcal{A}_{surv}(SPV3)}{\mathcal{A}_{surv}(SPV2)}\right]\left[\frac{\sigma_\epsilon(SPV3)}{\sigma_\epsilon(SPV2)}\right]^{-1}\left[\frac{n_g(SPV3)}{n_g(SPV2)}\right]^{-1/2} = 0.77$$

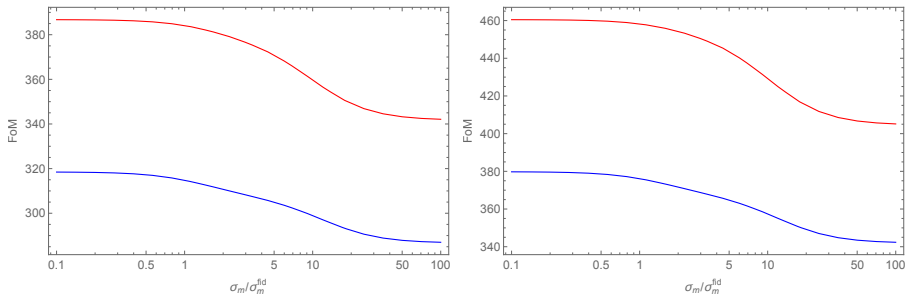

Figure 6: FoM as function of control parameter ε_m for 10 (left) and 13 (right) EP (blue) or ED (right) bins. The full Euc dataset is used here.

so that, scaling up, we predict FoM(SPV2) $\simeq 444$ in good agreement with the actual value FoM(SPV2) $\simeq 420$, the difference being due to the updated $n_i(z)$.

The choice of 13 ED bins may be considered conservative since it is based on the FoM value obtained after marginalising over all nuisance parameters with no prior. The right panel in Fig. 5 shows the same result when we instead add to the total Fisher matrix a prior matrix constructed according to Eq.(5) rules. As expected, there is a boost in the FoM which is approximately constant for $\mathcal{N}_{bin} \geq 10$. However, such an increase is not very significant being $\sim 10\%$ (12%) for EP (ED) bins. This is nevertheless enough to make the case with 11 ED bins able to pass the requirement on the FoM since it is FoM = 412 now.

It is worth focusing a bit more on the priors we have adopted. First, we have reduced the number of quantities to vary by assuming an equal prior for all the shear multiplicative bias parameters. As fiducial value, we have taken the upper limit in the requirement on m. However, this limit is actually not on the error on m, but on its actual value. That is to say, one is asking that the condition $|m| \leq 1.5 \times 10^{-3}$ is verified in order to not bias the estimate of the cosmological parameters, but this is not the same as saying that $\sigma(m) < 1.5 \times 10^{-3}$. A similar argument also holds for $\sigma_{pz}/(1+z)$ which is set to 0.005 as fiducial prior, while the requirement is actually $|\Delta z_i| \leq 0.005(1+z_i)$ rather than $\sigma(\Delta z_i) \leq 0.005(1+z_i)$. Motivated by these considerations, we have therefore investigated how, for a fixed number and type of bins, the FoM change as a function of $\varepsilon_m = \sigma(m_i)/\sigma_{fid}(m_i)$ and $\varepsilon_{pz} = \sigma(\Delta z_i)/\sigma_{fid}(\Delta z_i)$ with

$$\sigma_{fid}(m_i) = 1.5 \times 10^{-3} \quad , \quad \sigma_{fid}(\Delta z_i) = 0.005(1+z_i) \quad .$$

Note that, in general, both (ε_m) and ε_{pz} may depend on the redshift bin, but we take them equal for all bins to simplify the analysis. Fig. 6 shows the result of this analysis for the case with 10 or 13 redshift bins, either equiopulated or equidistant. The curves tend to flatten at the two extremes of the plotted range. On one hand, the FoM saturates as ε_m is very low since we approach more and more the case where the systematics are known with infinite precison, i.e. , they are fixed. At the opposite extreme, the prior on the systematics becomes so weak that we are in the situation with effectively no priors at all. The overall variation is, however, smaller than $10 - 12\%$ for a variation of $\sigma(m)/\sigma_{fid}(m)$ spanning three orders of magnitude. This could naively suggest that investing resources to improves the priors on the systematics nuisance parameters is a

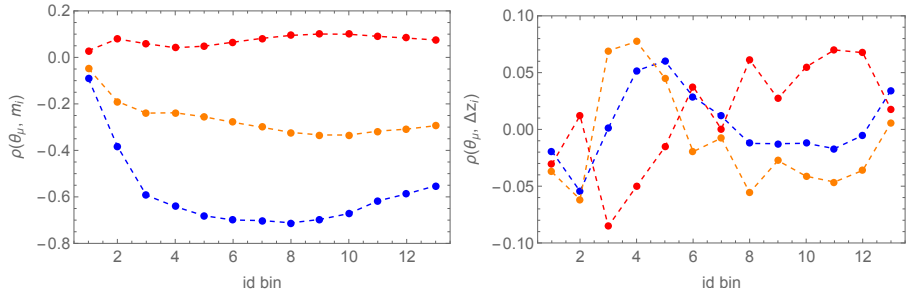

Figure 7: Correlation coefficients of the cosmological parameter θ_μ with the systematics m_i (left) and Δz_i (right) nuisance ones for the case with 13 ED bins. Blue, orange, and red lines refer to $\theta_\mu = (\Omega_M, w_0, w_a)$, respectively

worthyless exercise. However, the results in Fig. ,6 only tell half of the story. Indeed, they quantitfy the effect of priors on the accuracy, but one should also be confident that an incorrect determination of the fiducial systematics introduces a negligible bias in the estimate of the cosmological parameters. This can be quantified using the Fisher matrix formalism, but it is outside tour aims here.

In Fig. 6, we have set $\sigma(\Delta z_i)$ to its fiducial value. We have checked that the FoM is almost fully independent on how large is this prior. In order to understand this unexpected result, we can look at Fig. 7 where we plot the correlation coefficient of the cosmological parameters (Ω_M, w_0, w_a) with both m_i (left) and Δz_i (right) parameters as estimated from the Fisher matrix for the case with 13 ED bins. As it is evident, the shift parameters Δz_i have a negligible correlation with the cosmological ones, while the shear multiplicative bias m_i are strongly correlated with the matter density, and have a non negligible correlation with the dark energy equation of state quantities. This consideration explains why reducing the uncertainties on Δz_i does not affect the FoM since they do not break any degeneracy. The opposite effect happens for the shear multiplicative bias. We stress again, however, that a requirement on the value of Δz_i must be set in order to not shift the inferred cosmological parameters from their actual values. Quantifying this requirement is again outside our aim.

2.4 Constraining deviations from GR through γ

Euclid is aiming at detecting evidence for modified gravity (MG) too. A simple way to quantify it is looking at the growth index γ defined trhough the relation

$$f(z) = -\frac{d\ln D(z)}{d\ln(1+z)} \simeq [\Omega_M(z)]^\gamma \tag{10}$$

with $f(z)$ the growth rate, and $D(z)$ the growth factor. For GR, Eq.(10) provides an excellent fit to $f(z)$ with $\gamma = 0.55$ for the ΛCDM model. Detecting deviatons from this value is a signature for MG. Following the then available literature, in IST:F the effect of γ on the matter power spectrum was included setting

$$P_{mm}^{MG}(k,z) = \left[\frac{D_{MG}(z)}{D_{GR}(z)}\right]^2 P_{mm}^{GR}(k,z) \tag{11}$$

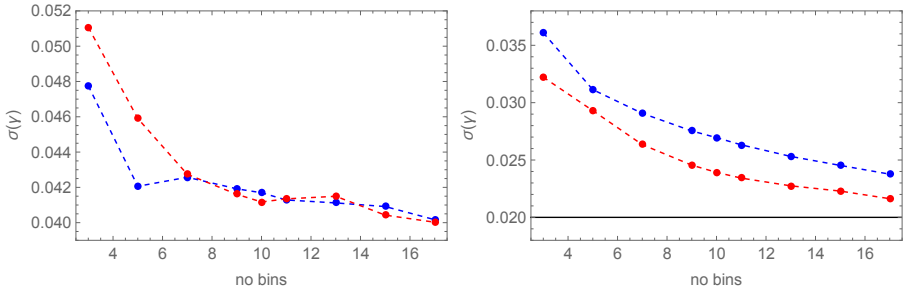

Figure 8: Marginalised constraints on the growth index γ using EP (blue) and ED (red) bins. Left and right panels refer to the results when priors on systematics are absent or present. The black horizontal line is the Red Book requirement.

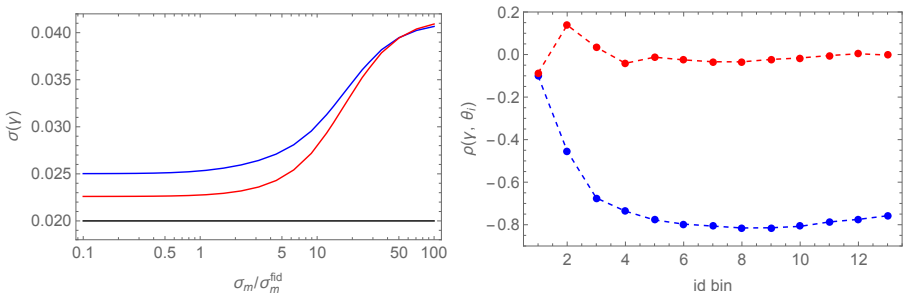

Figure 9: *Left.* Marginalised error on γ as a function of the prior on the shear multiplicative bias for the case with 13 EP (blue) and ED (red) bins and a fiducial prior on the mean redshift bias. *Right.* Correlation coefficient of γ with the m_i (blue) and Δz_i (red) nuisance parameters for the case with 13 ED bins.

where quantities with the label GR (MG) refers to the GR (MG) case, and the growth factor is obtained integrating Eq.(10) with the corresponding γ value. Eq.(11) is exact in the linear regime, but it was extrapolated to the nonlinear one too under the simplifying assumption that MG only changes the redshift dependent overall amplitude of the power spectrum in the same way at all scales. Today, it is well known that this is far from the truth yet we keep on using Eq.(11) in doing forecasts on γ in order to make a fair comparison with both IST:F and SPV2 results. We just note that it is actually possible to go beyond Eq.(11) and account for γ in a nonlinear recipe.

Using the linear recipe to modify accordingly all the power spectra of interest, we can easily get the constraints on γ in a non flat model. These are shown in Fig. 8 for EP (blue) and ED (red) bins after marginalising over all the other parameters without (left) and with (right) a prior on the systematics ones. Somewhat surprisingly, apart from the small $\mathcal{N}_{bin}$ regime, the constraints are roughly the same for both EP and ED bins. This is related to the strong correlation of γ with the nuisance parameters. Indeed, setting a prior on them, we partially break the degeneracy and get the same conclusion found when looking at the FoM, that is to say, ED bins are favoured with respect to EP ones. Unfortunately, however, the marginalised error on γ is larger than the Red Book requirement marked by the horinzontal black line in the right panel.

Narrowing down the prior on the shear multiplicative bias parameters does not help since we are already in the regime where no improvement can be obtained as shown in the left panel of Fig. 9. Note, however, that $\sigma(\gamma)$ has a strong dependence on $\varepsilon_m = \sigma(m)/\sigma_{fid}(m)$ with the constraint worsening, e.g., by a factor 1.8 for $\varepsilon_m = 100$. On the contrary, there is no dependence at all on $\sigma(\Delta z_i)$ so that the prior on the mean shift are of no relevance for the constraint on γ. This can again be explained looking at the strong correlation between γ and m_i shown by the blue curve in the right panel of Fig. 9 which also shows that γ is perfectly uncorrelated with Δz_i everywhere but for the first three bins having a yet small values of the correlation coefficient.

As a further attempt to fulfil the requirement, we have tried to be more optimistic in the usage of GCsp data. We increase the k_{max} to $0.30h$/Mpc still marginalising over the purity parameter. This has, however, a very minor impact on the constraints with $\sigma(\gamma)$ only decreasing from 0.0227 to 0.0221 for 13 ED bins and priors on systematics. We therefore conclude that the failure in meeting the Red Book value can be fully ascribed to the change in the survey specifics. Indeed, scaling $\sigma(\gamma)$ to the old values of $(\mathcal{A}_{surv}, \sigma_\epsilon, n_g)$, we get $\sigma(\gamma) = 0.020$ for 13 ED bins thus meeting the requirement.

3 Updating the recipe to `CLOE v2`

All the results presented above have been obtained using the same recipe for the observables used for IST:F and SPV2 forecasts and later implemented in `CLOE v1`, the only difference being the addition of the systematics as nuisance parameters. IST:L has now (almost) completed the implementation of a new recipe for both photometric and spectroscopic probes which has been included in (the next to be released) v2 of `CLOE`. Moroever, this same recipe (provided by the Likelihood WP of the WLSWG in accordance with the GCph WP of the GCSWG) has been implemented in `LiFE` so that it is possible to make 3x2pt forecasts based on it (while the GCsp Fisher matrix is still based on IST:F recipe apart for the marginalisation over the purity nuisance parameter). This is what we are going to do in the present section.

First, let us schematically remind what are the new ingredients included referring the interested reader to the `CLOE v2` documentation for details.

i. We include the ℓ-dependent prefactors which multiply the harmonic spectra due to projection of the derivatives opertor from curved to flat sky.

ii. We use a simplified description of the impact of redshift space distortion (RSD) on the GCph and GGL spectra which is valid under the assumption of linear and deterministic galaxy bias. The recipe adopted is rigorously valid in the linear regime only, while we extrapolate its validity in the nonlinear one too. However, on nonlinear scales, the RSD effect is largely negligible so that such extrapolation has no impact at all.

iii. We include the impact of magnification bias on both GCph and GGL adding the relevant terms to the corresponding harmonic power spectra. We fix the fiducial values of the magnification bias as described in Sect. 2.2

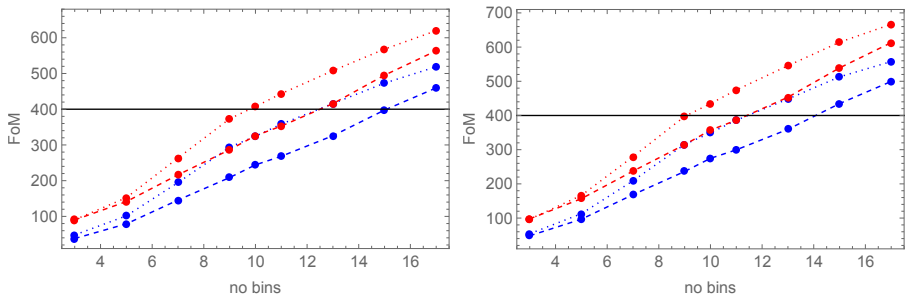

Figure 10: FoM vs number of EP (blue) and ED (red) bins for the non flat GR model using the updated `CLOE v2` recipe. Nuisance parameters are marginalised over without any priors in the left panel, while fiducial priors on systematics are used in the right panel. The horizontal line is the Red Boor requirement.

based on the slope of the number density - magnification threshold relation as measured from the Flagship mock data.

While the first two modifications only affect the low ℓ regime, magnification is present over the full multipole range. Moreover, the related additional terms can be of the same order as the density - density and density - shear ones which were the only contributions included in the IST:F recipe. In particular, depending on the sign of $b_M(z) = 5s(z) - 2$, the data vectors element corresponding to GCph and GGL can be very different and change sign with respect to the case with no magnification bias. The dramatic impact of magnification has been already discussed in the literature, and has been also presented in a recent Euclid Key Project paper of the GCph team. We therefore include it in the updated recipe also taking it into account when computing the analytic data covariance matrix.

Fig. 10 shows the total FoM (WL + GCph + GGL + GCsp + BOSS) as a function of the number of EP (blue) or ED (red) bins using or not priors on the systematics nuisance parameters. Notwithstanding the fact that the total number of parameters to constrain is now larger due to the presence of the $\mathcal{N}_{bin}$ magnification bias ones, the FoM is definitely larger than before for all the cases considered provided that $\mathcal{N}_{bin} \geq 7$ (5) for EP (ED) bins. As a consequence, the minimal number of bins needed to get FoM ≥ 400 is smaller than before. Indeed, we now find

$$\text{FoM} = \begin{cases} 415 & \text{for 13 EP bins} \\ \\ 407 & \text{for 10 ED bins} \end{cases}$$

if no priors on systematics are used, while it is

$$\text{FoM} = \begin{cases} 453 & \text{for 13 EP bins} \\ \\ 435 & \text{for 10 ED bins} \end{cases}$$

when fiducial priors are included.

These results come as a surprise since they are naively counterintuitive. Including magnification indeed increases the number of nuisance parameters so

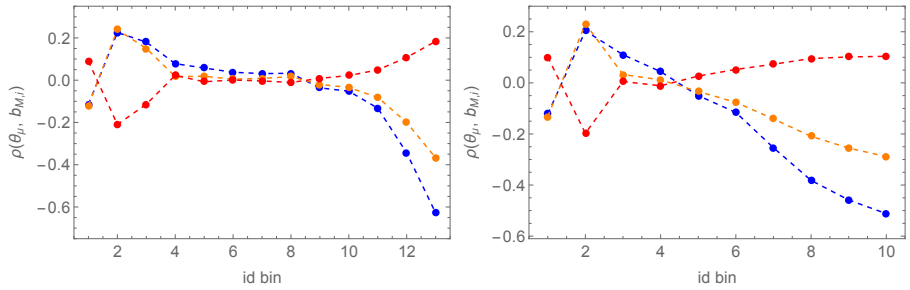

Figure 11: Correlation coefficents of Ω_M (blue), w_0 (orange), w_a (red) with the magnification bias parameters for the cases with 13 EP (left) and 10 ED (right) bins using the full Euc dataset to constrain a non flat GR model.

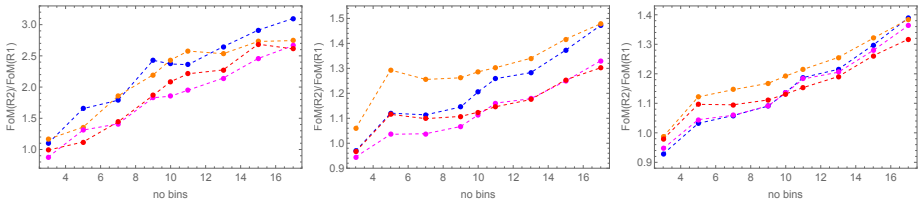

Figure 12: FoM ratio as function of the number of bins for GCO (left), All (centre), and Euc (right) datasets with FoM(R1) and FoM(R2) the FoM using IST:F and `CLOE v2` recipes, respectively. Blue (EP bins) and orange (ED bins) lines refer to marginalising over nuisance parameters with no priors, while a prior on systematics is included to get magenta (EP) and red (ED) ones.

there should be a reduction of the constraining power because of the possible opening up of new degeneracy direction in the multiparameter space. Fig. 11 shows that this is indeed happening, but not in a very dramatic way. The correlation coefficients of the magnification bias parameters with[6] (Ω_M, w_0, wa_a) is non negligible, but also not very large being $|\rho(\theta_\mu, b_{M,i})| \leq 0.2$ for most of the bins. As such, the reduction in the constraining power is less severe than what one may naively expect by simply counting the number of nuisance parameters.

A second consideration helpful to understand why the FoM is larger when including magnification can be guessed by looking at Fig. 12 where we plot the FoM ratio separating the probes. The most striking result is the large increase in the FoM for the case with using GCph data only. This can be understood going back to the expression of the Fisher matrix elements

$$F_{ij} = \left(\frac{\partial \mathcal{D}}{\partial \theta_\mu}\right)^T \cdot \Psi \cdot \left(\frac{\partial \mathcal{D}}{\partial \theta_\mu}\right) \ . \tag{12}$$

For the GCO dataset, the derivatives of the n-th element of the data vector are of the form

[6]We do not show the full set of cosmological parameters to avoid cluttering the plots with too many lines. However, these three parameters are the ones most involved in the determination of the FoM or more constrained by 3x2pt data.

$$\frac{\partial \mathcal{D}_n}{\partial \theta_\mu} = \frac{\partial C_{ij}^{GG}(\ell_k)}{\partial \theta_\mu}$$
$$= \frac{\partial C_{ij}^{\delta\delta}(\ell_k)}{\partial \theta_\mu} + \frac{\partial C_{ij}^{\delta\mu}(\ell_k)}{\partial \theta_\mu} + \frac{\partial C_{ij}^{\mu\delta}(\ell_k)}{\partial \theta_\mu} + \frac{\partial C_{ij}^{\mu\mu}(\ell_k)}{\partial \theta_\mu} \quad (13)$$

where (i, j, k) depend on n, and the terms $(\delta\delta, \delta\mu, \mu\delta, \mu\mu)$ refer to the density - density, density - magnification, magnification - density, and magnification - magnification contributions to the total GCph harmonic power spectrum. The last three terms are missing in the IST:F recipe, but they are far from being neglibile. As such, the derivatives of the GCO data vector are larger than before hence motivating the net increase in the FoM. A similar argument also holds for the GGL elements of the full 3x2pt data vector, while WL is not affected. Since the GCph is the least constraining probe if taken alone, it is clear that the impact of magnification is smoothed out as one keeps adding probes which have a stronger constraining power but are independent or less affected by magnification. The net effect is, however, still present explaining why we still get an overall increas of the FoM even if with smaller numbers on the y - axis of the central and rightmost panel in Fig. 12. The increasing trend with the number of bins is also a consequence of the additional terms in the derivatives since they affect more and more element of the Fisher matrix as $\mathcal{N}_{bin}$ gets larger.

We also note that an additional help in improving the FoM comes from the fact that, being the sign of the magnification bias negative in some bin combinations, some of the elements in the covariance matrix are smaller than in the no magnification case. Quantifying the net effect is, however, harder since it depends on too many possible combinations so we do not investigate it.

These considerations make us confident that our results are physically motivated hence reliable. As a further check, we have run a case with a intermediate recipe including magnification, but removing both the flat sky and RSD correction terms. We consider 13 bins and a flat GR model, and compare the improvement of the constraints on (w_0, w_a) from GCO data with the same numbers found in the magnification Key Project paper. The results agree within 15% which is quite satisfactory considering the differences in the number of multipole bins, the input matter power spectrum, and the way the derivatives of the data vectors are computed. Although not being a full validation challenge, this test further strenghten our belief in the results presented here .

We can then also look at the constraints on γ when we move from non flat GR to non flat MG model. Taking the two configurations which optimise the FoM, we get for the no priors case

$$\sigma(\gamma) = \begin{cases} 0.031 & \text{for 13 EP bins} \\ \\ 0.027 & \text{for 10 ED bins} \end{cases}$$

with an improvement of 22% and 32% with respect to the results using the IST:F recipe. The constraints are, however, still larger than the requirement. A significant help is obtained adding the priors on the systematics leading to

$$\sigma(\gamma) = \begin{cases} 0.025 & \text{for 13 EP bins} \\ \\ 0.023 & \text{for 10 ED bins} \end{cases}$$

which are, however, still larger than the requirement. We therefore must again conclude that the change in $(\mathcal{A}_{surv}, \sigma_\epsilon, n_g)$ degrades the constraints on γ in a way which makes it impossible to fulfil the original requirement.

4 Departure from the optimal scenario

According to the results in the previous sections, the minimal number of redshift bins needed to get FoM ≥ 400 depends on the recipe used. Since `CLOE v2` is the likelihood code which will be adopted to run MCMC based forecasts, we will hereafter consider as fiducial the results obtained using its recipe hence including the contribution by magnification. In this case, we must set

$$\mathcal{N}_{bin} \geq \begin{cases} 13 & \text{if EP bins are used} \\ \\ 10 & \text{if ED bins are used} \end{cases} , \tag{14}$$

where we have considered the case with no priors on the systematics to be conservative. These results have been obtained for what we are used to refer to as the *optimistic* scenario, i.e. assuming the data span the full range $(10, 5000)$ in multipoles (with cut on the GCph and GGL data vectors) and that all the galaxies in the redshift range $(0.001, 4.0)$ are included in the WL and GCph sample provided they pass the magnitude cut. In SPV2+, some of us investigated whether some of these assumptions could be dropped. This is the aim of the present section where we will use only the `CLOE v2` recipe, and consider the cases with $\mathcal{N}_{bins}$ larger than the mimimum value in Eq.(14).

4.1 Dependence on ℓ_{min}

Following common practice in recent data analyses and previous forecasts, we have set $\ell_{min} = 10$. However, on such large scales, the Limber approximation breaks down and the error due to its usage may propagate to the final constraints introducing a bias in the estimate of the cosmoloigical parameters. This has been shown to be negligible for WL data, while it can be important for GCph and GGL ones. Going beyond Limber approximation is not possible either with `CLOE v2` or `LiFE`. Although the implementation of post Limber is predicted for `CLOE v3`, it is expected that the computing time will significantly increase making harder to explore a large number of scenarios.

It is therefore worth wondering whether one can push ℓ_{min} to larger values thus avoiding the need of going beyond Limber. To this end, we here consider the FoM as function of ℓ_{min} in order to check whether we can increase ℓ_{min} without degrading the FoM itself.

This analysis is a work in progress at the moment. It is worth noticing, however, that, in SPV2+, we found that using $\ell_{min} = 50$ has not a serious impact on the FoM. We also stress that increasing ℓ_{min} makes the results more robust with respect to the RSD modeling since its impact becomes more and more negligible as we increase ℓ_{min}.

4.2 Dependence on the minumum redshift

In accordance with IST:F and SPV2 forecasts, we have included in the WL and GCph samples all galaxies passing the magnitude cut. However, it can be hard to reliably measure the photo - z of galaxies with $z < 0.2$ so that it is worth wondering whether we can drop the first bin without degrading the FoM. That this could indeed be the case is suggested by the fact that the S/N is smaller than in other bins. However, the first bin is also the one where the IA effect is more important so that dropping it can weaken the constraints on IA parameters and then propagate to those on cosmological ones because of degeneracy. Moreover, the first bin is the one where the impact of γ is larger since, in the highest redshift bins, $\Omega_M(z)$ approaches unity making it meaningless the actual value of γ. In SPV2+, we nevertheless found that one can set $z_{min} = 0.2$ without dramatic impact on the constraints. It is therefore worth repeating this analysis here with the updated recipe and survey specifics.

This analysis is in progress at the time of writing.

4.3 Dependence on k_{max}

Including in the data vector harmonic power spectra measured up to 3000 (5000) for GCph and GGL (WL) is actually a big act of faith on our ability to correctly estimate the matter power spectrum on scales as small as $k >$ few Mpc^{-1}. A naive way to reduce the impact of uncertainties on the nonliner recipe is to include in the data vector only elements evaluated in

$$\ell \leq \ell_{max}(z_i) = k_{max} r(\bar{z}_i) - 1/2$$

with $r(z_i)$ the comoving distance to the mean redshift $\bar{z}_i$ of the i - th bin. We investigate here the dependence on k_{max} looking for compromise between the need to get $FoM > 400$ and the possibility to model the power spectrum on small scales. We do not use the BNT formalism in order to better compare with the IST:F and SPV2 forecasts although this method is implemente in `CLOE v2`.

This analysis is again work in progress.

4.4 Impact of Super Sample Covariance

All of the above analysis has been done using an analytic covariance matrix for the photometric probes only including the Gaussian contribution. Again, this assumption has been made to compare with IST:F and SPV3 forecasts. We can nevertheless make more realistic forecasts letting the Super Sample Covariance (SSC) contribution enter the game. Although typically subdominant with respect to the Gaussian term for on diagonal covariane matrix elements, SSC plays a great role since it causes the off diagonal elements to be no more vanishing. As a consequence, data at different ℓ are now correlated thus reducing the effective number of degrees of freedom hence weakening the constraints. The results (soon to be submitted to ECEB) obtained in Key Project paper dedicated to this issue have shown that SSC dramatically impact the constraining power of WL, while it leaves almost unaltered the GCph one with GGL being in between these two extrema. The overall effect is a reduction of the FoM for

flat GR models by as much as 40% depending on the value of ℓ_{max}.

We are now in the phase of producing new SSC covarince matrices using an upadted version of the code developed by D. Sciotti and M. Bonici based on the `PySSC` *software by F. Lacasa and S. Goyou - Beauchamps with new response functions computed by V.F. Cardone. As soon as the Gauss + SSC covariance matrices will be ready, we will plug them into* `LiFE` *to compute new values of the FoM for the cases of most interest.*